Journal of Colloid and Interface Science 700 (2025) 138358

Contents lists available at ScienceDirect

Journal of Colloid And Interface Science

journal homepage: www.elsevier.com/locate/jcis

Phenolic terpenes in liposomal bilayers: Unraveling physicochemical interactions and membrane perturbation via biophysical and computational approaches

Serena Pilato [a,b], Simone Carradori [a], Francesco Melfi [a], Stefano Di Giacomo [a], Stefania Ciavarella [a], Michele Ciulla [a,b], Antonella Fontana [a,b], Pietro Di Profio [a], Massimiliano Aschi [c], Samanta Moffa [a,**], Gabriella Siani [a,b,*]

[a] Dipartimento di Farmacia, Università "G. d'Annunzio", via dei Vestini 31, 66100 Chieti, Italy
[b] UdA-TechLab, Research Center, Università degli Studi Gabriele d'Annunzio Chieti-Pescara, Via dei Vestini 31, 66100 Chieti, Italy
[c] Dipartimento di Scienze Fisiche e Chimiche, Università degli Studi dell'Aquila, via Vetoio, Coppito, 67100 L'Aquila, Italy

HIGHLIGHTS

- Thymol, carvacrol, and ether derivatives were successfully loaded into liposomes.
- Multiple biophysical analyses were employed to explore terpene-lipid interactions.
- DSC revealed perturbations in membrane phase behaviour.
- Raman spectroscopy offered molecular-level details on lipid-terpene interactions.
- Monoterpenes primarily interact at the headgroup and upper acyl chain regions.
- Phenolic monoterpenes enhance membrane permeability to encapsulated dye.
- The free hydroxyl group plays a key role in increasing membrane permeability.

GRAPHICAL ABSTRACT

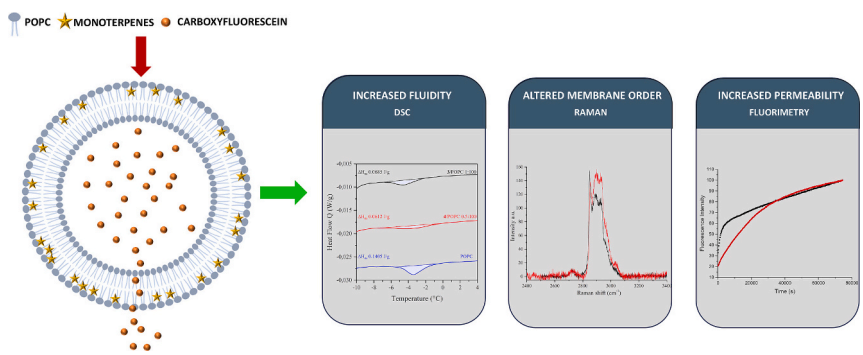

ARTICLE INFO

Keywords:
Liposomes
Terpenes
Differential scanning calorimetry
Raman spectroscopy

ABSTRACT

The interaction of small hydrophobic and amphiphilic molecules with lipid membranes plays a pivotal role in modulating membrane structure, dynamics, and permeability, which are key factors in applications ranging from drug delivery to antimicrobial design. In this study, we investigate the incorporation of the phenolic monoterpenes thymol and carvacrol, along with some ether derivatives, into unilamellar liposomes composed of 1-palmitoyl-2-oleoyl-*sn*-glycero-3-phosphocholine (POPC). These systems were prepared via the thin-film hydration method and characterized at two distinct terpene/lipid molar ratios. A comprehensive array of biophysical techniques was employed to elucidate the structural and thermotropic modifications induced by terpene incorporation. Dynamic light scattering (DLS) provided insights into vesicle size and colloidal stability. Differential Scanning Calorimetry (DSC) revealed perturbations in membrane phase behaviour, while Raman

* Corresponding author.
** Corresponding author.
E-mail addresses: samanta.moffa@unich.it (S. Moffa), gabriella.siani@unich.it (G. Siani).

https://doi.org/10.1016/j.jcis.2025.138358
Received 10 April 2025; Received in revised form 24 June 2025; Accepted 3 July 2025
Available online 4 July 2025
0021-9797/© 2025 The Authors. Published by Elsevier Inc. This is an open access article under the CC BY-NC-ND license (http://creativecommons.org/licenses/by-nc-nd/4.0/).

spectroscopy offered molecular-level details on lipid-terpene interactions, particularly at the headgroup and upper acyl chain regions.

Additionally, Molecular Dynamics simulations indicated a preferential localization of terpenes just beneath the lipid headgroup, further reinforcing the experimental observations. Fluorescence-based permeability assays using 5(6)-carboxyfluorescein (CF), interpreted through a biphasic kinetic model, showed that phenolic terpenes promoted membrane leakage, especially during the initial burst phase, suggesting a key role for the phenolic -OH group in mediating interfacial interactions.

This study advances our understanding of molecular determinants governing guest-bilayer interactions and underscores the utility of model membrane systems and complementary biophysical tools for probing structural phenomena in soft matter systems.

1. Introduction

Understanding the interactions between small amphiphilic or hydrophobic molecules and lipid bilayers is a central topic in colloid and interface science, with broad implications ranging from drug delivery and nanocarrier design to antimicrobial agent development and membrane biophysics [1–5].

Lipid membranes are dynamic soft interfaces characterized by a delicate balance between hydrophobic and polar interactions, whose perturbation by molecular guests can induce changes in membrane fluidity, permeability, phase behaviour, and domain formation [2,6–10]. Elucidating the underlying mechanisms of guest-bilayer interactions is thus essential for a predictive understanding of colloidal stability, transport properties, and functional performance in biological and biomimetic systems.

Model lipid bilayers, particularly unilamellar liposomes, provide a well-controlled environment for studying these interactions. As simplified analogues of biological membranes, liposomes allow precise control over composition, curvature, and thermodynamic parameters, making them ideal for systematic investigations of structure-property relationships [3]. Their versatility has led to widespread use both as drug delivery carriers for hydrophobic and hydrophilic molecules [11–13], and as in vitro models to study mechanisms and kinetics of molecular transport [14–18].

Advanced biophysical techniques such as dynamic light scattering (DLS), differential scanning calorimetry (DSC), and Raman spectroscopy provide quantitative insights into how guest molecules influence bilayer organization, thermotropic transitions, and mechanical stability. When combined with molecular dynamics (MD) simulations, these tools offer a comprehensive framework for interpreting complex behaviour at multiple scales, including guest localization preferences, the nature of interactions (e.g., hydrogen bonding or hydrophobic contacts), and the resulting impact on membrane organization and dynamics.

In this context, we investigate the interaction of the phenolic monoterpenes thymol (2-isopropyl-5-methylphenol) and carvacrol (5-isopropyl-2-methylphenol), along with selected ether derivatives (Fig. 1), with model membranes composed of 1-palmitoyl-2-oleoyl-*sn*-glycero-3-phosphocholine (POPC). Thymol and carvacrol, major components of essential oils from thyme (*Thymus vulgaris* L.) and oregano (*Origanum vulgare* L.), exhibit a wide range of biological activities,

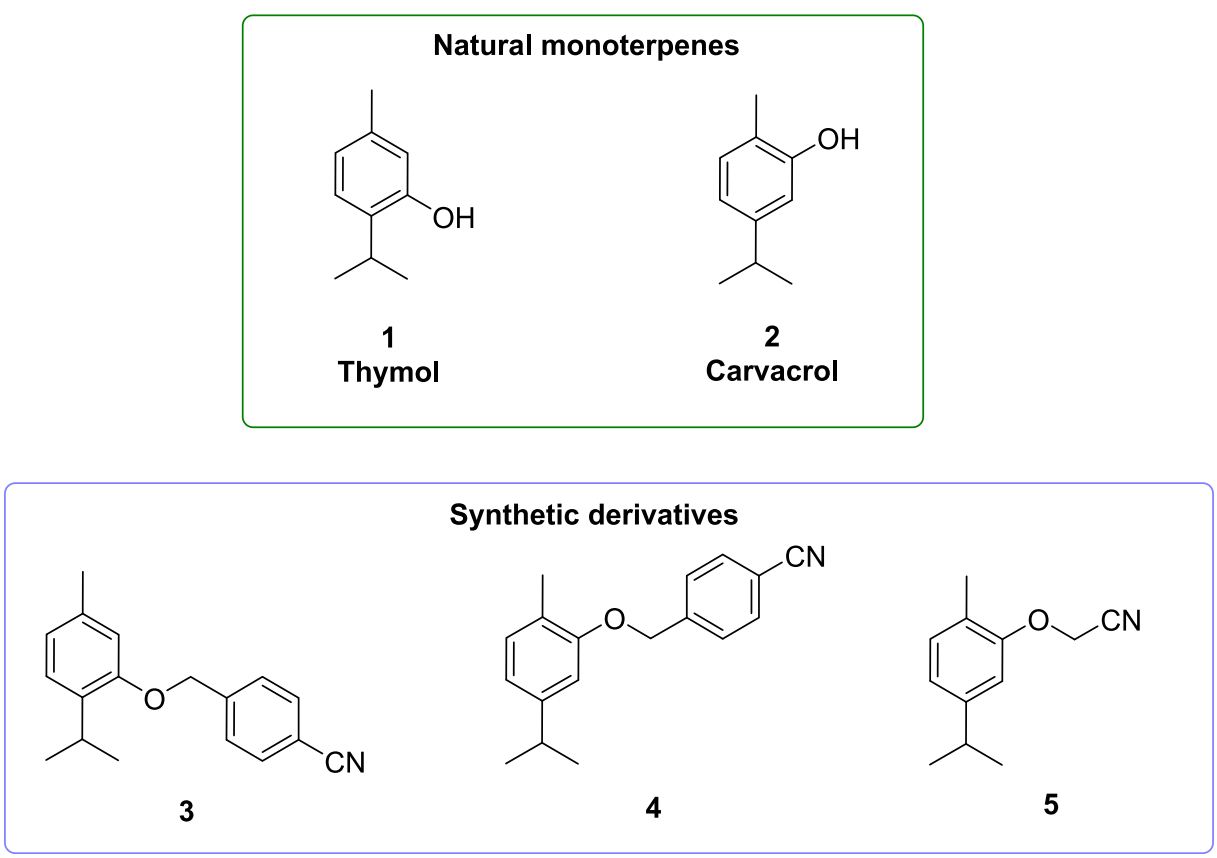

Fig. 1. Structures of the selected terpenes and derivatives.

including antiseptic, anti-inflammatory, antifungal, and antimicrobial effects, largely attributed to their interaction with bacterial membranes [19–29]. The antimicrobial action is believed to involve insertion and accumulation within lipid bilayers, causing alterations in membrane fluidity, lipid order, and permeability [27–30].

The membrane-disruptive potential of thymol and carvacrol is thought to arise from a combination of hydrophobic partitioning and hydrogen bonding at the lipid-water interface, particularly via the phenolic -OH group [27,29,30]. Modifying this group by replacing it with ether -OR substituents, alters polarity, hydrogen bonding capacity, and lipophilicity, potentially affecting membrane interactions and antimicrobial efficacy. Some ether derivatives retain activity, although the precise impact depends on the nature of the substituent [31,32].

This study focuses on elucidating the molecular basis of terpene-lipid bilayer interactions by investigating how subtle chemical modifications, specifically, the replacement of the phenolic -OH group with ether -OR groups, affect the incorporation, localization, and membrane-perturbing effects of thymol, carvacrol, and their derivatives in POPC liposomes. We applied a multi-technique strategy involving DLS to determine vesicle size and colloidal stability, DSC to monitor thermotropic behaviour, Raman spectroscopy to probe bilayer organization and terpene-lipid interactions, and fluorescence leakage assays to evaluate membrane permeability. By combining these experimental biophysical techniques with molecular dynamics simulations, we reveal that these monoterpenes preferentially interact with the polar headgroup region of the bilayer, inducing significant changes in membrane permeability and thermotropic behaviour without compromising vesicle integrity.

Our key findings demonstrate that the presence of a free hydroxyl group strongly enhances membrane permeability through increased leakage in the initial burst phase, while ether derivatives modulate this effect primarily at higher terpene-to-lipid ratios. These results highlight the critical role of specific molecular features in governing guest-bilayer interactions and their consequences for membrane structure and stability.

Notably, although POPC liposomes are widely used as model membranes, their thermotropic behaviour in the presence of small amphiphilic or hydrophobic molecules remains understudied by calorimetric methods. Our work represents one of the few comprehensive DSC analyses of POPC vesicles incorporating bioactive compounds, providing novel insights into the thermal stability and structural organization of these soft, self-assembled systems.

By connecting chemical structure with molecular behaviour at lipid interfaces, this study not only advances fundamental understanding of membrane-active agents but also offers a framework that could inform the rational design of bioactive materials with tailored membrane interactions for biomedical and antimicrobial applications.

2. Experimental

2.1. Chemicals and materials

1-Palmitoyl-2-oleoyl-*sn*-glycero-3-phosphocholine (POPC) was purchased from Avanti Polar Lipids (Alabaster, AL). The fluorescent probes 5(6)-carboxyfluorescein (CF), pyrene, thymol, carvacrol, $CHCl_3$, CH_3CH_2OH, Sephadex G-25, ethylene glycol and the salts used for the preparation of buffers were purchased from Sigma Aldrich and used without further purification. All chemicals used were of analytical grade, water was doubly distilled deionized of HPLC grade, and all experiments were conducted with freshly prepared solutions.

Compounds **3**–**5** were synthesized and purified according to published procedures [31,32]. In particular, they were obtained through a nucleophilic substitution reaction, by using 4-cyanobenzyl bromide for **3** and **4**, and 2-bromoacetonitrile for **5** [31,32].

2.2. Instruments

Fluorimetric measurements have been carried out on Jasco FP-6500 spectrofluorimeter. U*V*–vis spectra have been recorded by a Jasco *V*-550 UV/Vis spectrophotometer. The size and ζ potential values of liposomal systems were measured by using a 90Plus/BI-MAS ZetaPlus multiangle particle size analyzer (Brookhaven Instruments Corp., Holtsville, NY). DSC was conducted using an DSC25 (TA Instrument, New Castle, DE 19720, USA). Experiments were collected in the range of temperature from −15 °C to 25 °C, using a ramp of 1 °C/min. All data collection and manipulation were carried out using TA Instrument TRIOS (version 5.6.0.87).

Atomic Force Microscopy (AFM) measurements were carried out using a Multimode 8 system (Bruker, Billerica, MA, USA) equipped with a Nanoscope *V* controller, operating in ScanAsyst in air mode.

Raman spectra were collected by confocal and high-performance Raman microscope (XploRA PLUS, HORIBA, Japan) with deep-cooled CCD detector technology. LabSpec 6.6.1.14 (Horiba, Japan) was employed to control, optimize, and process the acquired data.

2.3. Computational details

Molecular dynamics simulations were performed with the program Gromacs version 5.0.4. [33]. The POPC membrane and all the species inserted in the membrane were described using a force-field obtained from Automated Topology Builder [34]. Water molecules were described using the Single Point Charge (spc) model [35]. All the simulations were carried out in the canonical ensemble; the temperature was kept fixed at 298 K using the velocity-rescale algorithm [36]; the Particle Mesh Ewald was used for the electrostatics [37] and all the bond lengths were kept frozen using the LINCS algorithm [38]. For each system we performed two simulations: the first one with the solute initially located in the water membrane interface; the second one with the solute inserted in the central part of the membrane. This strategy, which could only provide us with qualitative information, was selected in order to minimize uncertainties derived from the (relatively) long relaxation times. The simulations were carried out according to the following protocol: (i) the system was first minimized; (ii) the system was then gradually heated from 10 K to 298 K using short (500 ps) trajectories. (iii) Finally, the productive run was propagated up to 100.0 ns. For each system, 200 ns of simulation was utilized for the final results.

The trajectories were analyzed through simple home-made routines in particular following, along the simulation time, the position of the solute along the membrane.

2.4. Preparation of liposomal systems

Large POPC unilamellar vesicles have been prepared by the thin film hydration method, following the procedure reported in the literature [17]. Briefly, the appropriate amount of a guest stock solution in $CHCl_3$ has been added to a 25 mg/mL stock solution of POPC in $CHCl_3$ to give the desired final guest/lipid ratio (0.5:100 or 1:100). The mixture was evaporated at 40 °C under reduced pressure and the obtained thin lipid film formed on the wall of the flask was vacuum dried and rehydrated with MilliQ water or the appropriate aqueous buffer solution, depending on the type of measurement. After a hydration period of 30 min at room temperature, the lipid suspension was extruded at a nitrogen pressure of ~500 psi with 5 passes through polycarbonate membranes (pore size 200 nm, Nucleopore Track-Etched Membranes, Whatman, GE Healthcare, USA) mounted on an extruder (Lipex Biomembranes, Vancouver). The extrusion was performed at room temperature.

Spectrophotometric measurements were carried out to confirm the incorporation of guests into the liposomal bilayer. The UV–vis spectra of guests in CH_3OH and the spectra of the related hybrid liposomal systems are reported in Supplementary Materials (Fig. S1).

The amount of encapsulated guest was calculated as the difference between the total weighed amount of guest and the unincorporated fraction, which included the portion recovered from the polycarbonate membranes used during extrusion (washed with CH_3OH), as well as the fraction retained in the Sephadex during the gel-filtration step, subsequently eluted with CH_3OH. The recovered guest was quantified using a calibration curve. The encapsulation efficiency, EE, was calculated by Eq. 1:

$$EE\ (\%) = [(\text{total guest} - \text{unincorporated guest})/\text{total guest}]\ \text{x}\ 100\% \quad (1)$$

and was found to be ≥98 % for all guests.

2.5. Dynamic light scattering (DLS) analysis

For DLS measurements, the phospholipid thin film was rehydrated with MilliQ water. The mean hydrodynamic radius values and polydispersity indexes were obtained by analysing the scattering intensity autocorrelation function, assuming a log Gaussian distribution of the liposome size. DLS was also used to assess ζ potential values which were calculated from the electrophoretic mobility.

2.6. Atomic force microscopy (AFM) analysis

AFM was employed to examine the surface morphology and size characteristics of the POPC-based liposomal systems incorporating different guest molecules. For sample preparation, a drop of diluted liposome suspension (guest-to-lipid molar ratio of 1:100) was deposited onto SiO_2 substrates and subjected to controlled drying, initially at 303 K for 2 h in an oven, followed by overnight drying at room temperature. Imaging was performed in air using a ScanAsyst-Air silicon probe (triangular shape, resonance frequency ~ 70 kHz, nominal spring constant 0.4 N/m) operated in ScanAsyst mode. Topographic images (512 × 512 pixels) were recorded at a scan rate of 1 Hz with varying scan sizes and analyzed using Nanoscope Analysis 1.8 software.

2.7. Differential scanning calorimetry (DSC) experiments

Since the melting transition of ice overlap the gel-to-fluid phase transition temperature of POPC (T_m ~ −2 °C), the phospholipid thin film was rehydrated with an ethylene glycol/H_2O 30:70 *v*/v mixture, with a freezing point of ~ −14 °C. This protocol effectively prevented the interference caused by freezing water and revealed the phase transition of POPC. Indeed, ethylene glycol-based water solutions are commonly used in heat-transfer applications where the temperature in the heat transfer fluid can occur below 0 °C [39,40].

Approx. 25 μL of the liposomal suspension were loaded in a preweighed, hermetically sealed DSC pan. The reference pan was filled with the same components of the sample except the lipid phase. Samples were cooled from 25 °C to −15 °C and then warmed from −15 °C to 25 °C at a rate of 1 °C/min. The entire procedure was repeated to ensure reproducibility. All data used for analysis were taken from the heating scans, while cooling scans were used to check for hysteresis of the transitions. The thermal behaviour of liposomes was evaluated by determining the main transition temperature (T_m) and the enthalpy of the transition (ΔH_m) expressed as J/g of liposomes in the sample.

2.8. Raman experiments

A drop of suspension of pure POPC liposomes or guest-doped liposomes was deposited on a silicon wafer substrate. The Raman peaks were observed under a 532 nm laser with optical grating of 2400-line/mm. All spectra were collected in the spectral ranges 600–1600 cm^{-1} and 2000–3500 cm^{-1}, with the same measurement parameters (10s integration time, 15 accumulations, ~10 mW laser power at the sample surface) focusing on the surface, at the edge of the drop, with a 100× objective, to avoid laser-induced heating.

2.9. Fluorimetric measurements

The change in the bilayer microviscosity induced by the incorporation of the guests into the liposomal membrane has been determined fluorimetrically by using the environmentally sensitive fluorophore pyrene as the probe. The fluorescent intensity ratio I_E/I_M, where I_E is the fluorescent intensity of the excimer at λ = 480 nm and I_M is the fluorescent intensity of the monomer at λ = 395 nm, was used to estimate the membrane viscosity. The final concentrations of guests were 1.32 × 10^{-6} M (guest/lipid ratio = 0.5:100), and 2.64 × 10^{-6} M (guest/lipid ratio = 1:100). Experiments were carried out following a previously reported procedure [17]. Briefly, 1 μL of a stock solution 2 × 10^{-3} M of pyrene in ethanol was added directly to the cuvette containing the liposomal suspension every 3 min for a period of 30 min until a final concentration of pyrene of 1 × 10^{-5} M was reached, which ensures an adequate fluorescence intensity in all the experiments. The total amount of added ethanol never exceeds 0.5 % to avoid that high concentrations of ethanol could interfere with the organization of the acyl chains of the phospholipids inside the membrane [41]. The fluorescence emission spectrum was recorded after each addition of pyrene, using an excitation wavelength of 335 nm.

Content release experiments have been performed by using the fluorescent probe CF. The phospholipid thin film was rehydrated with a 50 mM CF solution in a buffer prepared from NaCl (121.5 mM), Na_2HPO_4 (25.2 mM) and KH_2PO_4 (4.8 mM). The CF concentration was chosen in order to achieve a quenching concentration in the inner aqueous core. The unentrapped dye was removed by passing the liposomal suspension through a Sephadex G-25 column at room temperature. The liposome suspension was then diluted with an isosmotic buffer (578 mOsm - pH 7.40) from NaCl (174 mM), Na_2HPO_4 (105 mM), and KH_2PO_4 (20 mM) to obtain a final POPC concentration of 1.32 × 10^{-5} M. The increase in fluorescence emission intensity at λ = 516 nm, using 490 nm as the excitation wavelength, due to the CF de-quenching which occurs after the leakage of the entrapped CF from the liposomes, was monitored over a period of 24 h.

3. Results and discussion

3.1. Computational analysis

As briefly described in the Computational Details section, we analyzed the position of the solute along the membrane for each system. The results are reported in the Fig. 2.

According to the reported values, Fig. 2 clearly shows that our simulation setup indicates that, essentially in all the investigated cases, the solute preferentially resides within the solvent-membrane interface.

Interestingly the width of the distributions also suggests that, essentially in all the investigated cases, the solutes are rather mobile. In one case (compound **4**) the solute also appears as able to reach, with low but non-zero probability, the core of the membrane. As already remarked in the Computational Details section, our results do not allow a fully quantitative picture and, hence, the small differences observed in the reported distributions are probably not significant. It follows that the only conclusion that can realistically and irrefutably be reached is that all the species appear to preferentially occupy the solvent-membrane interface.

3.2. Characterization of hybrid liposomal systems

3.2.1. Particle size and zeta potential

Particle size and zeta potential are valuable sources of information on the physicochemical changes that occur in a lipid bilayer when a guest is incorporated into the membrane. Indeed, the insertion of a guest molecules into the liposomal bilayer can promote phospholipid

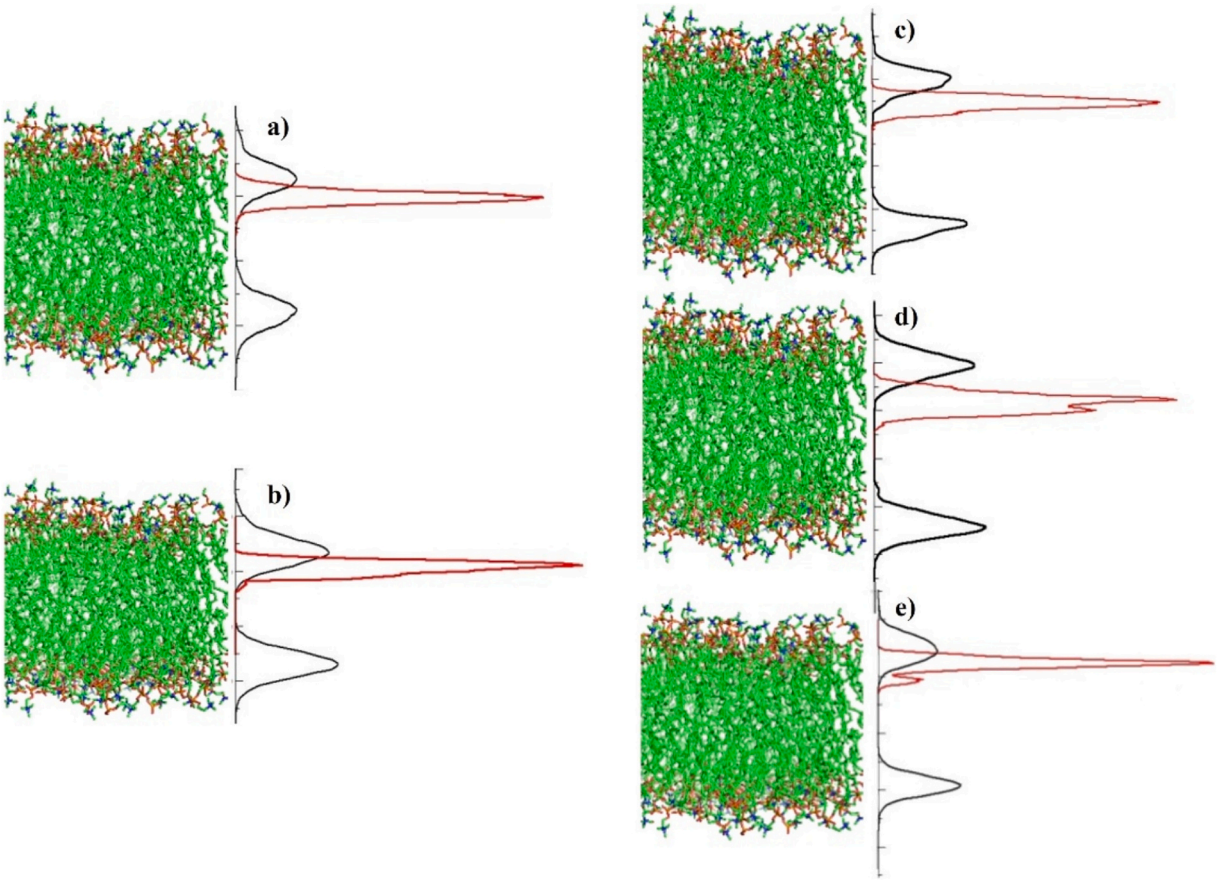

Fig. 2. Distributions of the solute centre-of-mass (red) and membrane polar heads (black) for a) **1**/POPC, b) **2**/POPC, c) **3**/POPC, d) **4**/POPC, e) **5**/POPC systems. Data are averaged over two trajectories with maximum deviations not exceeding 2.0 Å. (For interpretation of the references to colour in this figure legend, the reader is referred to the web version of this article.)

rearrangement by altering the morphology of liposomes as well as the physicochemical properties of the liposomal surface. The effect of the insertion of the studied guests on the POPC liposome morphology was evaluated by DLS analysis in terms of mean hydrodynamic diameter, and the surface charge of the liposome was quantified by measuring the ζ potential. The polydispersity index was also determined to assess the distribution of the liposome population, specifically the homogeneity of particle sizes. The results obtained for the hybrid liposomal systems, along with those for pure POPC liposomes for comparison, are reported in the Supplementary Material (Tables S1-S3).

DLS analysis confirmed the presence of particles whose diameters are consistent with the existence of liposomal aggregates, suggesting that the insertion of the guests did not affect substantially the structural integrity of liposomes, which is maintained after guest loading. The polydispersity index values indicate a relatively homogeneous size distribution. However, the size of hybrid systems was found to change, compared to pure POPC liposomes, suggesting that, even if liposome structure is not disrupted, the presence of the guests influence the curvature of the membrane. Measurements of ζ-potential provide a quantitative assessment of liposomal phosphate group surface exposure in the presence of guest molecules by analysing the liposomal surface charge. The negative surface charge of the liposomes increases upon guest insertion (Table S3). This result suggests that the guests predominantly localize near the polar head groups of the phospholipids, influencing their orientation and enhancing their exposure at the interface. A similar shift in ζ-potential values has been observed in DPPC liposomal bilayers containing certain polyphenolic compounds [42], for which thermal analysis and ^{31}P NMR studies have confirmed their localization near the glycerol and C1-C10 region of the DPPC acyl chains. The same study suggested that molecules positioned closer to the bilayer center, from C10 onward, do not influence phosphate group exposure [42].

ζ potential values also quantify the degree of repulsion between charged particles in the dispersion. The high absolute values of the ζ potential obtained for the studied liposomes indicate a strong charge repulsion between the particles, that avoids their aggregation and precipitation, suggesting a high kinetic stability of the hybrid systems [43,44].

The stability of the liposomal formulations was evaluated at 0, 7, 14, and 21 days using dynamic light scattering (DLS) to monitor particle size and polydispersity index (PDI). The analysis was performed on samples stored at 4 °C in the dark. Over the 21-day storage period, DLS measurements revealed non-linear and fluctuating trends in both particle size and PDI across all liposomal systems, including pure POPC liposomes (Tables S1-S2), showing no evidence of large-scale aggregation or fusion and no clear tendency toward narrowing or broadening of the size distribution. Rather than indicating progressive destabilization, these fluctuations suggest a system in dynamic equilibrium and highlight the behaviour of the liposomal systems, which preserve their structural integrity despite minor, reversible changes in size and distribution.

3.2.2. AFM analysis

AFM imaging is well-suited for assessing the size and shape of heterogeneous systems such as liposome suspensions. Representative 2D height images of diluted pure POPC liposomes and POPC liposomes loaded with guest **1** are shown in Fig. 3.

Most vesicles exhibit a globular and somewhat flattened appearance, likely resulting from deformation during the drying process. It is worth noting that while AFM offers detailed morphological insights, particle

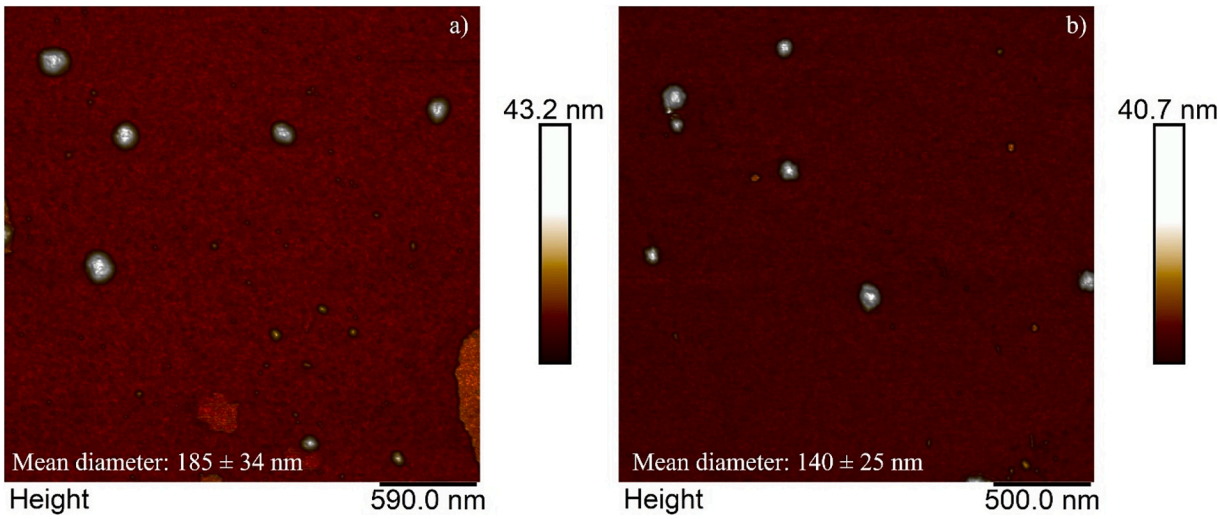

Fig. 3. AFM topography image of a) pure POPC liposomes and b) **1**/POPC liposomes (guest-to-lipid molar ratio = 1:100). AFM images of the other liposomal systems are provided in the Supplementary Material.

size estimates may be influenced by tip convolution, sample preparation artifacts, and the smaller number of vesicles analyzed, making it more reliable for qualitative assessment of vesicle shape and surface characteristics.

3.2.3. *Determining the microviscosity*

Fluorescence spectroscopy is a valuable technique for obtaining information on the structural order and, consequently, the microviscosity of bilayers. This method is based on the motion characteristics of pyrene in the membrane, since the ratio between the fluorescence intensity of the excimer (I_E) at 480 nm and the fluorescence intensity of the monomer (I_M) at 395 nm is determined by the diffusion-controlled collision frequency between laterally diffusing monomers, which is sensitive to the viscosity changes in the phospholipid membrane [45]. When the environment limits lateral diffusion of pyrene molecules, fluorescence emission originates from pyrene monomers while, when lateral diffusion is unrestricted, the pyrene monomers collide to form excimer whose fluorescence prevails in the emission spectrum. As an example, the fluorescence spectra of pyrene in the **3**/POPC liposomal system (guest/lipid ratio = 0.5:100) are shown in Fig. 4.

The parameter C'h, given by the equation.

$$C'h = (1/k)\eta$$

where k is a constant accounting for both theoretical and instrumental factors and η represents viscosity, was determined as the inverse of the slope of the linear plot of the I_{480}/I_{395} ratio versus pyrene

Table 1
C'h parameters calculated for pure POPC liposomes and hybrid liposomal systems.

	C'h (x 10^{-5})	
pure POPC [15]	15.9 (± 0.01)	
Liposomal system	Guest/POPC ratio 0.5:100	Guest/POPC ratio 1:100
1/POPC	6.93 ± 0.10	6.70 ± 0.43
2/POPC	8.00 ± 0.37	7.58 ± 0.34
3/POPC	7.50 ± 0.13	7.46 ± 0.01
4/POPC	8.05 ± 0.36	7.27 ± 0.21
5/POPC	8.61 ± 0.04	8.39 ± 0.02

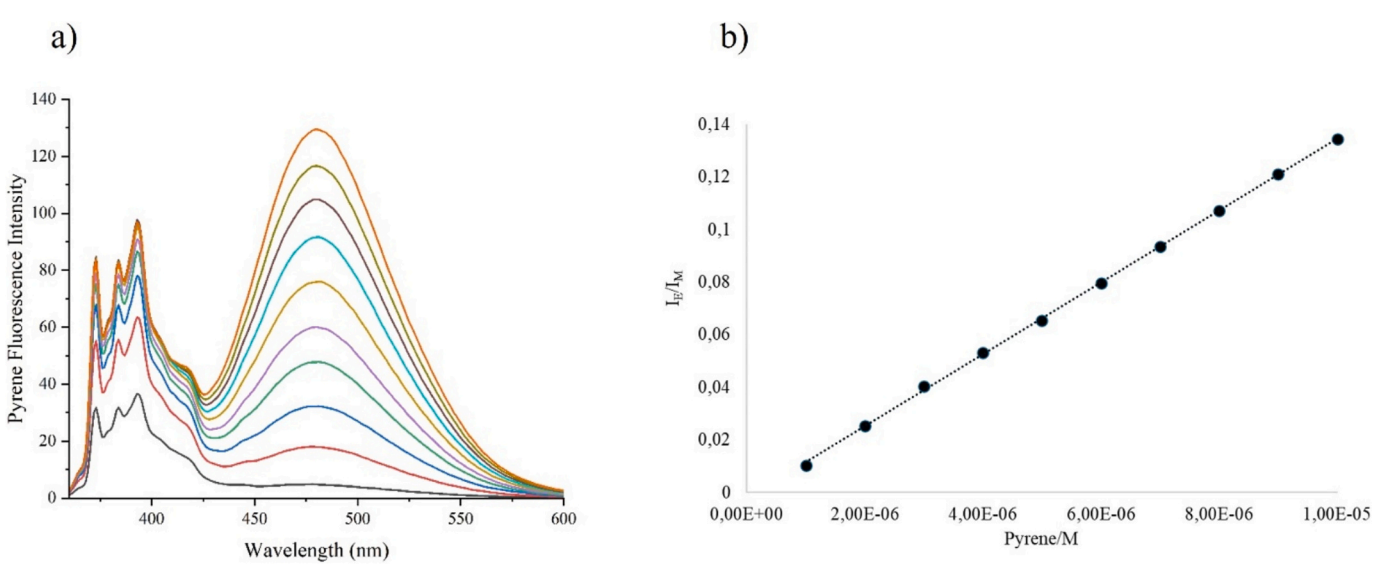

Fig. 4. a) Fluorescent emission spectra of pyrene in the liposomal system **3**/POPC (guest/lipid ratio = 0.5:100) registered at 1×10^{-6} M ≤ [pyrene] ≤ 1×10^{-5} M and b) plot of the $I_{E(480)}/I_{M(395)}$ ratio versus pyrene concentration.

concentration (Fig. 4b) and is presented in Table 1 as an indirect indicator of bilayer microviscosity for all the studied liposomal systems.

The data presented in Table 1 indicate that the incorporation of the different monoterpenes into POPC liposomes modifies the lipid membrane dynamic properties, leading to an increased fluidity, compared to pure POPC liposomes.

3.2.4. DSC analysis

Phospholipid membranes exhibit lyotropic properties, meaning they can exist in different phases, gel and liquid crystal, depending on temperature [46]. The transition between these phases, known as the gel-to-liquid crystal phase transition, is characterized by a transition temperature (T_m) and an associated enthalpy change (ΔH_m) which is determined by integrating the area under the calorimetric curve. Below T_m, in the gel phase, phospholipid aliphatic chains are tightly packed, oriented parallel in the *trans* configuration, and exhibit limited mobility. Above T_m, in the liquid crystalline phase, these chains adopt a more disordered state, increasing their mobility and shifting to a *gauche* conformation. The transition from an ordered to a disordered state requires heat absorption, which appears as an endothermic peak in the DSC curve.

Representative DSC thermograms are presented in Fig. 5.

As shown in Fig. 5, the liposomal bilayer of pure POPC liposomes displayed a typical peak at about −3.4 °C due to the transition from a gel to a liquid crystalline phase. This value is consistent with those reported in the literature, which typically range between −2 and − 5 °C [47–50].

Changes in DSC profiles were observed upon insertion of **1**–**5** into the liposomal bilayer, suggesting that guests modulate the organization and dynamics of the membrane and affect its overall thermodynamic behaviour. Guest insertion led to peak broadening and reduction in transition enthalpy compared to pure POPC control liposomes, while T_m showed a slight decrease, which became more pronounced at the highest concentrations of ether derivatives **3**–**5**. All thermodynamic parameters are listed in Table 2.

The broadening of the transition peak indicates that the guest molecule is situated in the C1 - C10 methylene region, where it interacts with the cooperative unit [42]. This interaction disrupts lipid packing and increases heterogeneity in the head group region, leading to a broader and less distinct endothermic peak due to a less cooperative phase transition which becomes less pronounced and occurs over a wider temperature range. In contrast, if a guest molecule is positioned closer to the bilayer center (C10 - C16 methylene region), the cooperative unit remains unaffected, resulting in a sharper transition peak. These findings correlate with the effect of guests on ζ-potential values which has been attributed to their localization in the C1 - C10 region of the POPC acyl chains.

The slight change in T_m coupled with a decrease in enthalpy upon guest insertion into the liposomal bilayer can be explained by the

Table 2
Thermotropic parameters obtained from the DSC profiles of pure POPC liposomes and guest/POPC liposomal systems.

Liposomal system	T_m (°C)	ΔH_m (J/g)
POPC	−3.42 ± 0.04	0.1390 ± 0.0116
1/POPC 0.5:100	−3.42 ± 0.05	0.0934 ± 0.0478
2/POPC 0.5:100	−3.76 ± 0.09	0.1130 ± 0.0105
3/POPC 0.5:100	−3.56 ± 0.17	0.0729 ± 0.0088
4/POPC 0.5:100	−3.67 ± 0.16	0.0614 ± 0.0066
5/POPC 0.5:100	−3.64 ± 0.11	0.0617 ± 0.0095
1/POPC 1:100	−3.71 ± 0.11	0.1008 ± 0.0140
2/POPC 1:100	−3.39 ± 0.07	0.1109 ± 0.0099
3/POPC 1:100	−4.54 ± 0.06	0.0717 ± 0.0082
4/POPC 1:100	−4.04 ± 0.13	0.0829 ± 0.0148
5/POPC 1:100	−4.17 ± 0.18	0.0920 ± 0.0130

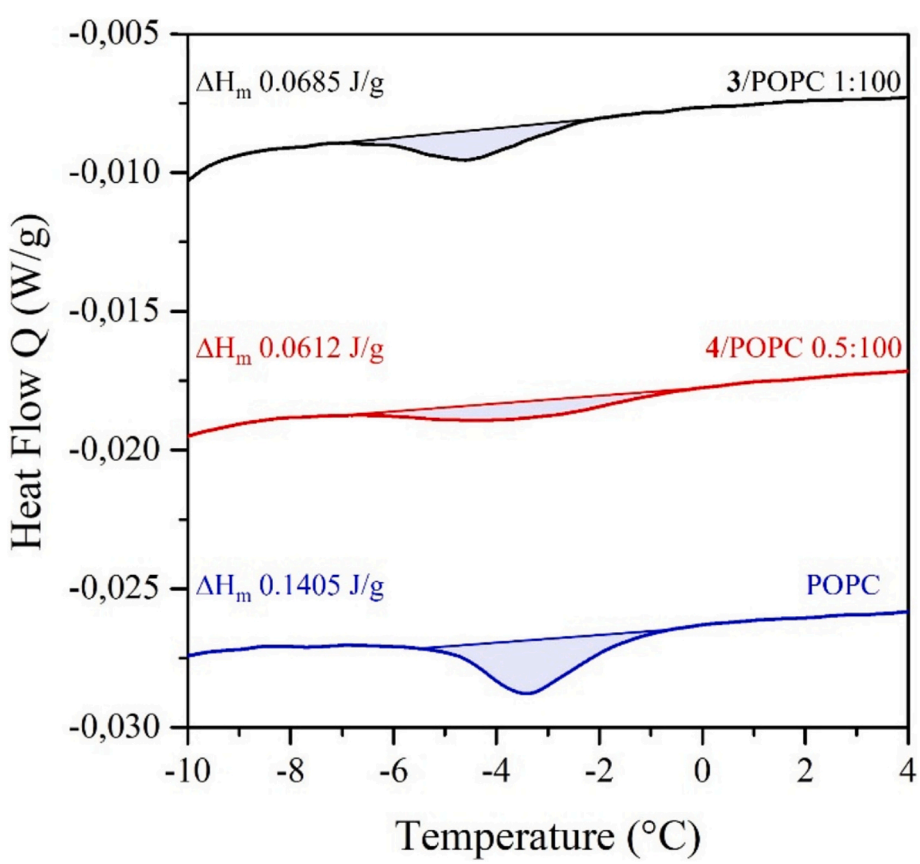

Fig. 5. DSC profiles of the gel-to-fluid state transition of pure POPC liposomes (blue line), **4**/POPC liposomal system 0.5:100 (red line) and **3**/POPC liposomal system 1:100 (black line). (For interpretation of the references to colour in this figure legend, the reader is referred to the web version of this article.)

location of the guest within the lipid structure. T_m reflects the cooperativity of the gel-to-liquid crystalline phase transition, which depends on the hydrophobic core's structural integrity. Guest molecules with limited ability to penetrate deeply into the hydrophobic core of the bilayers have a limited influence on T_m [51]. However, the interaction of the guest molecule with the polar head groups could weaken the cohesive forces between lipid molecules, leading to a less thermal energy required to shift from an ordered lipid packing to a more disordered state. As a result, despite their preferential location near the bilayer's polar head groups, guests may induce a shift to a more fluid state in the hydrophobic region of the bilayer. This interpretation aligns with ζ-potential measurements and computational analysis. At guest/POPC ratio 1:100, ether derivatives **3**–**5** demonstrated a greater effect on T_m. At this concentration, these guests, which lack a free OH group, likely disrupt the packing of the lipid chains more effectively.

The relevance of the DSC results obtained in this study is further underscored by the limited availability of calorimetric investigations on fully hydrated POPC liposomes interacting with small molecules. We identified only one study in which POPC vesicles were analyzed in the presence of a lipophilic guest, α-tocopherol, at physiological concentration (0.3 mol%) [52]. In that case, a slight reduction in both the main phase transition temperature (from −4.8 °C to −5.2 °C) and transition enthalpy was observed, suggesting perturbations at the interfacial level of the bilayer. Similarly, our data suggest that the terpene derivatives interact mainly with the polar headgroup region, as supported by complementary techniques and molecular dynamics simulations. This congruence further reinforces the robustness of our experimental setup. In contrast, other studies reporting calorimetric analysis of guest-lipid interactions typically involve dehydrated or partially hydrated POPC membranes, conditions not directly comparable to our fully hydrated systems [53,54]. In this context, our results further extend current knowledge by providing a detailed comparative analysis of different terpene structures, an aspect still largely unexplored for POPC in the hydrated state.

3.2.5. Raman analysis

Raman spectroscopy is a powerful analytical spectroscopic technique for obtaining molecular-level information on the structural organization and dynamics of lipid membranes. It is particularly useful for determining the localization of guest molecules within liposomal membranes [55]. By analysing specific spectral regions, Raman spectroscopy helps identify molecular interactions and structural perturbations induced by the incorporation of these molecules into the bilayer. The spectral region between 2800 cm^{-1} and 3050 cm^{-1} is crucial for assessing the structural and dynamic properties of phospholipid acyl chains inside the bilayer. This region contains three well-defined peaks that correspond to different vibrational modes of C—H bonds in the lipid tails: a peak at 2850 cm^{-1} assigned to the symmetric stretching of C—H bonds in methylene (-CH_2) groups, a peak at 2880 cm^{-1} assigned to the asymmetric stretching of C—H bonds in methylene (-CH_2) groups, and a peak at 2930 cm^{-1} assigned to the symmetric stretching of terminal C—H bonds in methyl (-CH_3) groups [56]. If a guest molecule is located in the hydrophobic domain of the membrane, it can alter the conformation and organization of lipid tails, leading to measurable changes in this spectral region [57]. The intensity ratios I_{2930}/I_{2850} and I_{2930}/I_{2880} are particularly informative because they are sensitive to the lateral packing density of the acyl chains. Changes in these ratios provide insight into how tightly the lipids are packed and whether the lipid tails adopt an ordered or disordered conformation [58]. Increase in I_{2930}/I_{2850} and I_{2930}/I_{2880} suggests a more disordered and fluid membrane, indicative of reduced lipid packing. Another key Raman spectral marker is the absorption band at 715 cm^{-1}, which is assigned to the symmetric stretching of the C—N bond in the choline moiety of the POPC head group. This vibrational mode is highly sensitive to molecular interactions occurring at the polar interface of the membrane: variations in the intensity or frequency of this peak serve as direct indicators of molecular interactions at the membrane interface, providing crucial information on whether a compound prefers to locate near the polar headgroups or to be embedded deeply within the bilayer [59]. Reduced choline C—N vibrational intensity may indicate disruption of lipid headgroup organization, possibly due to guest intercalation or competition with lipid-lipid interactions. It may also suggest increased membrane fluidity or destabilization.

By combining the analysis of both spectral regions (2800–3050 cm^{-1} for acyl chains and 715 cm^{-1} for head groups), the preferred localization of a guest molecule within the liposomal membrane can be determined. The Raman spectrum of POPC and of the hybrid liposomal systems were recorded and processed using Origin 2024, applying a 2nd derivative baseline correction. Deconvolution of the 2800–3050 cm^{-1} and 715 cm^{-1} regions in the Raman spectra was performed using Lorentzian peak fitting to resolve overlapping peaks into individual components and provide more precise information on the interactions between guest molecules and membrane phospholipids. [60] The interchain lateral ordering of the lipid molecules were characterized by the height intensity ratios I_{2930}/I_{2850} and I_{2930}/I_{2880}. As the integrated intensity of the CH_2 bending vibration peak near 1440 cm^{-1} is considered to be independent of the conformational change in the polar head [61], the intensity ratio I_{715}/I_{1440} was used to quantify changes in the C—N symmetric stretching vibration of the liposomal head choline group. A complete listing of peak intensity ratios is provided in Table 3, showing that changes occurred in both spectral regions.

The increase in I_{2930}/I_{2850} ratio and the decrease in I_{715}/I_{1440} ratio suggest that guest molecules, preferentially localized within the interfacial domain, simultaneously interact with phospholipid headgroups and the adjacent segments of hydrophobic tails. This interpretation aligns with ζ-potential measurements, DSC data and computational results. Additional evidence of guest interactions at the bilayer's polar head region is provided by a 2–4.4 cm^{-1} shift to a higher wavenumber in the C—N stretching peak of the Raman spectra for guest-loaded liposomes compared to pure POPC liposomes.

The limited impact on the I_{2930}/I_{2880} intensity ratio, particularly observed for guests **1** and **2**, and more generally for all guests at the lowest guest/lipid ratio, is more difficult to interpret. It could be inferred that, in these cases, the effect on packing primarily arises from an increase in rotational disorder and freedom of motion, which is reflected in the I_{2930}/I_{2850} ratio, rather than from a decrease in both intramolecular and intermolecular interactions, which are captured by the I_{2930}/I_{2880} ratio [62].

Consistent with the DSC results, guests **3**–**5**, at the highest concentration, showed the greatest effect on the interchain lateral ordering of lipid molecules.

3.3. Release experiments

Liposomal membrane permeability was assessed by monitoring the spontaneous release of the fluorescent probe CF from the aqueous core

Table 3
Peak intensity ratios calculated from Raman spectra of the investigated hybrid liposomal systems and pure POPC liposomes.

Liposomal system	I_{2930}/I_{2850}	I_{2930}/I_{2880}	I_{714}/I_{1440}
POPC	0.74 ± 0.06	0.89 ± 0.02	0.53 ± 0.01
1/POPC 0.5:100	0.81 ± 0.01	0.83 ± 0.04	0.49 ± 0.01
2/POPC 0.5:100	0.74 ± 0.03	0.86 ± 0.07	0.45 ± 0.01
3/POPC 0.5:100	0.87 ± 0.04	0.95 ± 0.02	0.43 ± 0.01
4/POPC 0.5:100	0.83 ± 0.02	0.88 ± 0.01	0.47 ± 0.03
5/POPC 0.5:100	0.89 ± 0.01	0.89 ± 0.05	0.45 ± 0.01
1/POPC 1:100	0.86 ± 0.01	0.83 ± 0.03	0.36 ± 0.02
2/POPC 1:100	0.75 ± 0.06	0.86 ± 0.01	0.35 ± 0.03
3/POPC 1:100	1.16 ± 0.01	1.01 ± 0.09	0.43 ± 0.01
4/POPC 1:100	1.08 ± 0.01	0.97 ± 0.01	0.39 ± 0.02
5/POPC 1:100	0.85 ± 0.01	0.97 ± 0.01	0.49 ± 0.01

of the aggregates. The release of CF, likely caused by pore formation and defects in the phospholipid bilayer [63], was tracked by measuring fluorescence intensity. CF fluorescence is quenched at high concentrations in the inner core of liposomes but increases (de-quenches) upon dilution in the external solution. Representative kinetic profiles of CF release from select liposomal systems are presented in Fig. 6.

The release behaviour follows a biphasic kinetic model with high accuracy, as indicated by correlation coefficients (R^2) $\geq$ 0.998, demonstrating excellent fit quality. This model describes liposomal content release as occurring in two distinct phases, each characterized by different rate constants. It captures heterogeneous release mechanisms, typically consisting of an initial rapid phase followed by a slower, sustained release. The general equation for biphasic release is:

$$[CF]_{eq} - [CF]_t = Ae^{-t/k_1} + Be^{-t/k_2} \quad (2)$$

where $[CF]_{eq}$ and $[CF]_t$ are the total concentrations of CF released at equilibrium and at time t, respectively, and k_1 and k_2 are the rate constants for the first and the second release step, respectively.

The fast release step represents the initial burst release of liposome content, possibly due to transient pore formation and/or defects in the lipid bilayer. The slow-release phase corresponds to the gradual diffusion of encapsulated content from the liposome core, potentially influenced by bilayer integrity or membrane restructuring.

Kinetic data presented in Table 4 indicate that thymol (**1**) and carvacrol (**2**) accelerate CF release during the initial "burst" phase. A similar effect is observed for derivatives **3–5** at the highest guest/lipid ratio. However, for derivatives **3**–**5** at the lowest guest/POPC ratio, the burst phase disappears, profiles display a more regular trait, and the first-order kinetic model provides the best fit for CF release (see Fig. 4).

Overall, the ability of the guest molecule to enhance membrane permeability appears to depend primarily on the presence of a free OH group and, to a lesser extent, on their concentration in the bilayer. This may be due to the stronger interaction of the free hydroxyl groups in compounds **1** and **2** with the membrane's polar region compared to the ether groups in compounds **3**–**5**, which disrupts the polar head organization and promotes pore or channel formation, thereby increasing permeability.

Table 4
Rate constant values for the biphasic (k_1 and k_2) and first-order (k_{obs}) release of CF from the investigated liposomal systems.

Lyposomal system	10^{-4} k_1 (s^{-1})	10^{-4} k_2 (s^{-1})	10^{-4} k_{obs} (s^{-1})
POPC	1.87 ± 0.03	0.257 ± 0.005	
1/POPC 0.5:100	4.39 ± 0.12	0.0725 ± 0.1323	
2/POPC 0.5:100	6.72 ± 0.39	0.0525 ± 0.0015	
3/POPC 0.5:100	–	–	0.426 ± 0.009
4/POPC 0.5:100	–	–	0.489 ± 0.001
5/POPC 0.5:100	–	–	0.356 ± 0.005
1/POPC 1:100	5.24 ± 0.13	0.0549 ± 0.0692	
2/POPC 1:100	9.33 ± 0.11	0.0735 ± 0.0007	
3/POPC 1:100	3.52 ± 0.96	0.183 ± 0.080	
4/POPC 1:100	3.08 ± 0.02	0.145 ± 0.002	
5/POPC 1:100	5.92 ± 0.01	0.240 ± 0.029	

3.4. Comparative discussion of the applied techniques

The combined use of DLS, ζ-potential, fluorescence spectroscopy, DSC, and Raman spectroscopy provides a consistent picture of how guest molecules modulate liposomal structure and dynamics. DLS and ζ-potential measurements suggest that guest insertion does not compromise liposome integrity but alters surface charge and curvature, pointing to preferential localization near the polar headgroups. This is supported by Raman spectral shifts and reduced intensity of the C—N choline vibration, indicating disruption at the membrane interface. Microviscosity data and Raman intensity ratios (I_{2930}/I_{2850}, I_{2930}/I_{2880}) reveal increased membrane fluidity and reduced lipid packing, especially for compounds with free hydroxyl groups (**1** and **2**). These findings correlate with DSC thermograms, where broadened transitions and decreased enthalpy reflect reduced cooperativity and increased bilayer disorder. The thermal and spectroscopic evidence consistently place guest

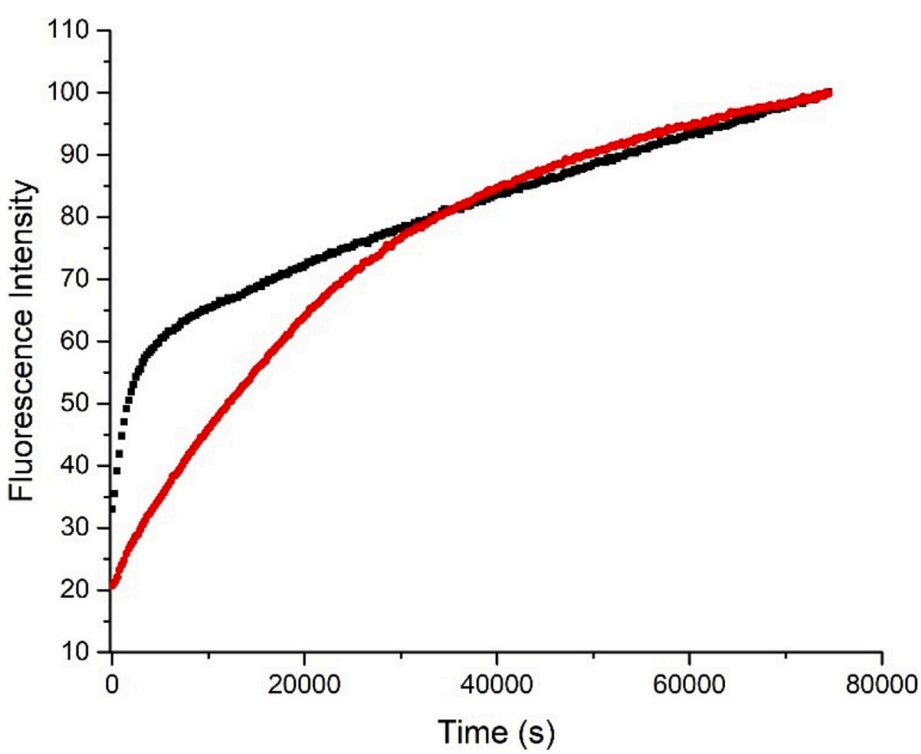

Fig. 6. Normalized kinetic profiles of the spontaneous CF release at 25 °C from **1**/POPC 0.5:100 (black line) and **5**/POPC 0.5:100 (red line) liposomal systems. (For interpretation of the references to colour in this figure legend, the reader is referred to the web version of this article.)

molecules within the C1-C10 region of the acyl chains. Release experiments confirm these structural effects functionally, with compounds **1** and **2** markedly enhancing membrane permeability. Overall, the integrated results from all techniques highlight a shared mechanism in which guest-membrane interactions occur primarily at the interface, leading to altered surface charge, packing, and bilayer fluidity.

4. Conclusions

This study provides a comprehensive and multi-scale analysis of the interactions between thymol, carvacrol, and their ether derivatives with biomimetic POPC liposomal membranes, aiming to unveil the molecular basis governing terpene–lipid interplay. All compounds were successfully incorporated into the bilayer with high encapsulation efficiency and without compromising liposome integrity, as confirmed by DLS and AFM. The absence of vesicle disruption suggests that these small hydrophobic guests are compatible with the lipid architecture at the concentrations tested.

A combination of biophysical techniques, including fluorescence leakage assays, differential scanning calorimetry, and Raman spectroscopy, revealed that the monoterpenes interact predominantly with the polar headgroup region of the bilayer, rather than penetrating deeply into the hydrophobic core. Notably, DSC studies on POPC liposomes remain limited in the literature; therefore, our thermotropic analysis offers novel insights into how these fluid-phase membranes respond to small guest molecules. These interactions led to measurable changes in membrane permeability and thermotropic behaviour. The presence of a free hydroxyl group in thymol and carvacrol significantly enhanced membrane permeability, as evidenced by increased CF release during the initial burst phase. In contrast, ether derivatives produced pronounced effects on the fast release step only at higher terpene-to-lipid ratios. Molecular dynamics simulations supported these experimental findings by confirming the preferential terpene localization beneath the polar interface.

By elucidating how minor chemical modifications in small guest molecules translate into distinct functional outcomes at the membrane level, this work advances our fundamental understanding of guest–bilayer interactions in soft matter systems. Beyond model membranes, our insights hold translational relevance for the rational engineering of liposomal drug delivery platforms, particularly in the design of systems with tunable permeability, stability, and release kinetics. As such, this study not only deepens the mechanistic knowledge of terpene-lipid dynamics but also contributes meaningfully to the development of more effective and predictable nanocarrier systems in biomedical applications.

CRediT authorship contribution statement

Serena Pilato: Methodology, Investigation, Data curation. **Simone Carradori:** Investigation. **Francesco Melfi:** Investigation. **Stefano Di Giacomo:** Investigation. **Stefania Ciavarella:** Investigation. **Michele Ciulla:** Visualization. **Antonella Fontana:** Funding acquisition, Data curation. **Pietro Di Profio:** Validation. **Massimiliano Aschi:** Writing – original draft, Investigation, Formal analysis. **Samanta Moffa:** Methodology, Investigation, Data curation. **Gabriella Siani:** Writing – original draft, Supervision, Conceptualization.

Declaration of competing interest

The authors declare the following financial interests/personal relationships which may be considered as potential competing interests: Serena Pilato reports financial support was provided by Italian Ministry of University and Research. Samanta Moffa reports financial support was provided by Italian Ministry of University and Research. Antonella Fontana reports financial support was provided by Italian Ministry of University and Research. Stefano Di Giacomo reports financial support was provided by Italian Ministry of University and Research. Stefano Di Giacomo reports financial support was provided by Carbotech srl Italy. If there are other authors, they declare that they have no known competing financial interests or personal relationships that could have appeared to influence the work reported in this paper.

Acknowledgements

S.P., A.F., S.M. acknowledges financial support funded by the European Union – NextGenerationEU, Mission 4, Component 2, under the Italian Ministry and Research (MUR) National Innovation Ecosystem Grant ECS 00000041 – Vitality – CUP D73C22000840006. S. D. G. was attending the PhD programme in “Scienze biomolecolari e farmaceutiche” at the University of Chieti-Pescara, Cycle XXXVIII, with the support of a scholarship co-financed by the Ministerial Decree no. 352 of 9th April 2022, based on the NRRP - funded by the European Union – NextGenerationEU - Mission 4 “Education and Research”, Component 2 “From Research to Business”, Investment 3.3, and by the company Carbotech S.r.l., via dell’industria, Martinsicuro (TE).

Appendix A. Supplementary data

Supplementary data to this article can be found online at https://doi.org/10.1016/j.jcis.2025.138358.

Data availability

Data will be made available on request.

References

[1] C. Peetla, A. Stine, V. Labhasetwar, Biophysical interactions with model lipid membranes: applications in drug discovery and drug delivery, Mol. Pharm. 6 (2009) 1264–1276, https://doi.org/10.1021/mp9000662.
[2] D. Lombardo, P. Calandra, D. Barreca, S. Magazù, M.A. Kiselev, Soft interaction in liposome Nanocarriers for therapeutic drug delivery, Nanomaterials 6 (2016) 125, https://doi.org/10.3390/nano6070125.
[3] S. Andrade, M.J. Ramalho, J.A. Loureiro, M. Carmo Pereira, Liposomes as biomembrane models: biophysical techniques for drug-membrane interaction studies, J. Mol. Liq. 334 (2021) 116141, https://doi.org/10.1016/j.molliq.2021.116141.
[4] S. Sekowski, N. Naziris, M. Chountoulesi, E. Olchowik-Grabarek, K. Czerkas, A. Veiko, N. Abdulladjanova, C. Demetzos, M. Zamaraeva, Interaction of *Rhus typhina* tannin with lipid nanoparticles: Implication for the formulation of a tannin–liposome hybrid biomaterial with antibacterial activity, J. Funct. Biomater. 14 (2023) 296, https://doi.org/10.3390/jfb14060296.
[5] O. Yu Selyutina, E.A. Shelepova, E.D. Paramonova, L.A. Kichigina, S.S. Khalikov, N. E. Polyakov, Glycyrrhizin-induced changes in phospholipid dynamics studied by 1H NMR and MD simulation, Arch. Biochem. Biophys. 686 (2020) 108368, https://doi.org/10.1016/j.abb.2020.108368.
[6] K. Sofińska, D. Lupa, A. Chachaj-Brekiesz, M. Czaja, J. Kobierski, S. Seweryn, K. Skirlińska-Nosek, M. Szymonski, N. Wilkosz, A. Wnętrzak, E. Lipiec, Revealing local molecular distribution, orientation, phase separation, and formation of domains in artificial lipid layers: towards comprehensive characterization of biological membranes, Adv. Colloid Interf. Sci. 301 (2022) 102614, https://doi.org/10.1016/j.cis.2022.102614.
[7] V.K. Sharma, E. Mamontov, Multiscale lipid membrane dynamics as revealed by neutron spectroscopy, Prog. Lipid Res. 87 (2022) 101179, https://doi.org/10.1016/j.plipres.2022.101179.
[8] K. Przykaza, M. Jurak, A.E. Wiącek, Effect of naproxen on the model lipid membrane formed on the water-chitosan subphase, BBA-Biomembranes 1865 (2023) 184099, https://doi.org/10.1016/j.bbamem.2022.184099.
[9] R. Wang, J. Peng, X. Shi, S. Cao, Y. Xu, G. Xiao, C. Li, BBA-Biomembranes 1864 (2022) 184015, https://doi.org/10.1016/j.bbamem.2022.184015.
[10] J. Gudyka, J. Ceja-Vega, K. Ivanchenko, W. Perla, C. Poust, A. Gamez Hernandez, C. Clarke, S. Silverberg, E. Perez, S. Lee, J. Phys. Chem. B 128 (2024) 2412–2424, https://doi.org/10.1021/acs.jpcb.3c08390.
[11] R. Kesharwani, P. Jaiswal, D.K. Patel, P.K. Yadav, Lipid-based drug delivery system (LBDDS): an emerging paradigm to enhance Oral bioavailability of poorly soluble drugs, Biomed. Mater. Devices 1 (2023) 648–663, https://doi.org/10.1007/s44174-022-00041-0.
[12] S. Losada-Barreiro, S. Celik, Z. Sezgin-Bayindir, S. Bravo-Fernández, C. Bravo-Díaz, Carrier Systems for Advanced Drug Delivery: improving drug solubility/bioavailability and administration routes, Pharmaceutics 16 (2024) 852, https://doi.org/10.3390/pharmaceutics16070852.

[13] B. Rocha, L.A. de Morais, M.C. Viana, G. Carneiro, Promising strategies for improving oral bioavailability of poor water-soluble drugs, Expert Opin. Drug Discov. 18 (2023) 615–627, https://doi.org/10.1080/17460441.2023.2211801.

[14] R. Zappacosta, G. Siani, S. Silvi, A. Credi, A. Fontana, Light-driven directed proton transport across the liposomal membrane, Langmuir 30 (2014) 13667–13672, https://doi.org/10.1021/la503604e.

[15] S. Pilato, M. Aschi, M. Bazzoni, F. Cester Bonati, G. Cera, S. Moffa, V. Canale, M. Ciulla, A. Secchi, A. Arduini, A. Fontana, G. Siani, Calixarene-based artificial ionophores for chloride transport across natural liposomal bilayer: synthesis, structure-function relationships, and computational study, BBA-Biomembranes 2021 (1863) 183667, https://doi.org/10.1016/j.bbamem.2021.183667.

[16] S. Moffa, S. Carradori, F. Melfi, A. Fontana, M. Ciulla, P. Di Profio, M. Aschi, R. D. Wolicki, S. Pilato, G. Siani, Fine-tuning of membrane permeability by reversible photoisomerization of aryl-azo derivatives of thymol embedded in lipid nanoparticles, Colloids Surf. B: Biointerfaces 241 (2024) 114043, https://doi.org/10.1016/j.colsurfb.2024.114043.

[17] R. Zappacosta, M. Aschi, A. Ammazzalorso, P. Di Profio, A. Fontana, G. Siani, Embedding calix[4]resorcinarenes in liposomes: experimental and computational investigation of the effect of resorcinarene inclusion on liposome properties and stability, BBA-Biomembranes 1861 (2019) 1252–1259, https://doi.org/10.1016/j.bbamem.2019.04.010.

[18] M. Orlikowska, A. Wyciszkiewicz, K. Węgrzyn, J. Mehringer, D. de Souza Paiva, P. Jurczak, Methods for monitoring protein-membrane binding. Comparison based on the interactions between amyloidogenic protein human cystatin C and phospholipid liposomes, Int. J. Biol. Macromol. 278 (2024) 134889, https://doi.org/10.1016/j.ijbiomac.2024.134889.

[19] O. Kosakowska, Z. Węglarz, S. Styczyńska, A. Synowiec, M. Gniewosz, K. Bączek, Activity of common thyme (*Thymus vulgaris* L.), greek oregano (*Origanum vulgare* L. ssp. hirtum), and common oregano (*Origanum vulgare* L. ssp. vulgare) essential oils against selected phytopathogens, Molecules *29* (**2024**) 4617, https://doi.org/10.3390/molecules29194617.

[20] R. Nurzyńska-Wierdak, M. Walasek-Janusz, Chemical composition, biological activity, and potential uses of oregano (*Origanum vulgare* L.) and oregano essential oil, Pharmaceuticals 18 (2025) 267, https://doi.org/10.3390/ph18020267.

[21] L.A. Sampaio, L. Tairiny Santos Pina, M. Russo Serafini, D. dos Santos Tavares, A. Gibara Guimarães, Antitumor effects of Carvacrol and thymol: a systematic review, Front. Pharmacol. 12 (2021) 702487, https://doi.org/10.3389/fphar.2021.702487.

[22] Y. Chang, W. Boukari, S.S. Riley, P.F. Harmon, A. Sarkhosh, J.K. Brecht, In vitro antifungal activity of white thyme, oregano, and savory oils against five *Monilinia fructicola* isolates from the southeastern United States, Plant Health Prog. 25 (2024) 262–269, https://doi.org/10.1094/PHP-12-23-0111-RSResearch.

[23] E. Vassiliou, O. Awoleye, A. Davis, S. Mishra, Anti-inflammatory and antimicrobial properties of thyme oil and its Main constituents, Int. J. Mol. Sci. 24 (2023) 6936, https://doi.org/10.3390/ijms24086936.

[24] Y. Hao, J. Li, L. Shi, A Carvacrol-rich essential oil extracted from oregano (*Origanum vulgare* "hot & Spicy") exerts potent antibacterial effects against *Staphylococcus aur*eus, Front. Microbiol. 12 (2021) 741861, https://doi.org/10.3389/fmicb.2021.741861.

[25] S. Mechmechani, A. Gharsallaoui, A. Fadel, K. El Omari, S. Khelissa, M. Hamze, N.-E. Chihib, Microencapsulation of carvacrol as an efficient tool to fight *Pseudomonas aeruginosa* and *Enterococcus faecalis* biofilms, PLoS One 17 (2022) e0270200, https://doi.org/10.1371/journal.pone.0270200.

[26] J.-H. Lee, Y.-G. Kim, J. Lee, Carvacrol-rich oregano oil and thymol-rich thyme red oil inhibit biofilm formation and the virulence of uropathogenic *Escherichia coli*, J. Appl. Microbiol. 123 (2017) 1420–1428, https://doi.org/10.1111/jam.13602.

[27] K. Kachur, Z. Suntres, The antibacterial properties of phenolic isomers, carvacrol and thymol, Crit. Rev. Food Sci. Nutr. 60 (2020) 3042–3053, https://doi.org/10.1080/10408398.2019.1675585.

[28] J. Xu, F. Zhou, B.-P. Ji, R.-S. Pei, N. Xu, The antibacterial mechanism of carvacrol and thymol against *Escherichia coli*, Lett. Appl. Microbiol. 47 (2008) 174–179, https://doi.org/10.1111/j.1472-765X.2008.02407.x.

[29] N.M. Wijesundara, S.F. Lee, Z. Cheng, R. Davidson, D.N. Langelaan, H.P. Vasantha Rupasinghe, Bactericidal activity of Carvacrol against *Streptococcus pyogenes* involves alteration of membrane fluidity and integrity through interaction with membrane phospholipids, Pharmaceutics 14 (2022) 1992, https://doi.org/10.3390/pharmaceutics14101992.

[30] A. Ultee, M.H.J. Bennik, R. Moezelaar, The phenolic hydroxyl group of carvacrol is essential for action against the food-borne pathogen *Bacillus cereus*, Appl. Environ. Microbiol. 68 (2002) 1561–1568, https://doi.org/10.1128/AEM.68.4.1561-1568.2002.

[31] F. Sisto, S. Carradori, P. Guglielmi, C.B. Traversi, M. Spano, A.P. Sobolev, D. Secci, M.C. Di Marcantonio, E. Haloci, R. Grande, G. Mincione, Synthesis and biological evaluation of carvacrol-based derivatives as dual inhibitors of *H. pylori* strains and AGS cell proliferation, Pharmaceuticals 13 (2020) 405, https://doi.org/10.3390/ph13110405.

[32] F. Sisto, S. Carradori, P. Guglielmi, M. Spano, D. Secci, A. Granese, A.P. Sobolev, R. Grande, C. Campestre, M.C. Di Marcantonio, G. Mincione, Synthesis and evaluation of thymol-based synthetic derivatives as dual-action inhibitors against different strains of *H. pylori* and AGS cell line, Molecules 26 (2021) 1829, https://doi.org/10.3390/molecules26071829.

[33] M.J. Abraham, D. van der Spoel, E. Lindahl, B. Hess, the GROMACS development team, GROMACS User Manual version 5.0.4. www.gromacs.org, 2014.

[34] A.K. Malde, L. Zuo, M. Breeze, M. Stroet, D. Poger, P.C. Nair, C. Oostenbrink, A. E. Mark, An automated force field topology builder (ATB) and repository: version 1.0, J. Chem. Theory Comput. 7 (2011) 4026–4037, https://doi.org/10.1021/ct200196m.

[35] H.J.C. Berendsen, J.P.M. Postma, W.F. van Gunsteren, J. Hermans, in: B. Pullman (Ed.), Intermolecular Forces, Reidel, Dordrecht, 1981, p. 331.

[36] G. Bussi, D. Donadio, M. Parrinello, Canonical sampling through velocity rescale, J. Chem. Phys. 126 (2007) 014101, https://doi.org/10.1063/1.2408420.

[37] T. Darden, D. York, L. Pedersen, Particle mesh Ewald: an N ·log(N) method for Ewald sums in large systems, J. Chem. Phys. 98 (1993) 10089–10092, https://doi.org/10.1063/1.464397.

[38] B. Hess, H. Bekker, H.J.C. Berendsen, J.G.E.M. Fraaije, LINCS: a linear constraint solver for molecular simulations, J. Comput. Chem. 18 (1997) 1463–1472, https://doi.org/10.1002/jcc.540181207.

[39] P.J. Davis, K.M.W. Keough, Phase diagrams of bilayers of dimyristoyl lecithin plus heteroacid lecithins, Chem. Phys. Lipids 35 (1984) 299–308, https://doi.org/10.1016/0009-3084(84)90072-0.

[40] https://www.engineeringtoolbox.com/ethylene-glycol-d_146.html.

[41] H.A. Pillman, G.J. Blanchard, Effects of ethanol on the organization of phosphocholine lipid bilayers, J. Phys. Chem. B 114 (2010) 3840–3846, https://doi.org/10.1021/jp910897t.

[42] S.A. Malekar, A.L. Sarode, A.C. Bach II, D.R. Worthen, The localization of phenolic compounds in liposomal bilayers and their effects on surface characteristics and colloidal stability, AAPS PharmSciTech 17 (2016) 1468–1476, https://doi.org/10.1208/s12249-016-0483-5.

[43] A. Wiącek, E. Chibowski, Zeta potential, effective diameter and multimodal size distribution in oil/water emulsion, Colloids Surf. A Physicochem. Eng. Asp. 159 (1999) 253–261, https://doi.org/10.1016/S0927-7757(99)00281-2.

[44] S. Moffa, M. Aschi, M. Bazzoni, F. Cester Bonati, A. Secchi, P. Bruni, P. Di Profio, A. Fontana, S. Pilato, G. Siani, Synthesis, characterization, and computational study of aggregates from amphiphilic calix[6]arenes. Effect of encapsulation on degradation kinetics of curcumin, J. Mol. Liq. 368 (2022) 120731, https://doi.org/10.1016/j.molliq.2022.120731.

[45] J. Vanderkooi, J. Callis, B. Chance, Use of the fluorescent dye, pyrene, to study the dynamic aspects of membrane structure, Histochem. J. 6 (1974) 301–310, https://doi.org/10.1007/BF01312248.

[46] D. Marsh, General features of phospholipid phase transitions, Chem. Phys. Lipids 57 (1991) 109–120, https://doi.org/10.1016/0009-3084(91)90071-I.

[47] W. Curatolo, B. Sears, L.J. Neuringer, A calorimetry and deuterium NMR study of mixed model membranes of l-palmitoyl-2-oleylphosphatidylcholine and saturated phosphatidylcholines, Biochim. Biophys. Acta Biomembr. 817 (1985) 261–270, https://doi.org/10.1016/0005-2736(85)90027-6.

[48] M. Fidorra, T. Heimburg, L.A. Bagatolli, Direct visualization of the lateral structure of porcine brain Cerebrosides/POPC mixtures in presence and absence of cholesterol, Biophys. J. 97 (2009) 142–154, https://doi.org/10.1016/j.bpj.2009.03.060.

[49] P.J. Davis, B.D. Fleming, K.P. Coolbear, K.M.W. Keough, Gel to liquid-crystalline transition temperatures of water dispersions of two pairs of positional isomers of unsaturated mixed-acid phosphatidylcholines, Biochem 20 (1981) 3633–3636, https://doi.org/10.1021/bi00515a051.

[50] J.A. Svetlovics, S.A. Wheaten, P.F. Almeida, Phase separation and fluctuations in mixtures of a saturated and an unsaturated phospholipid, Biophys. J. 102 (2012) 2526–2535, https://doi.org/10.1016/j.bpj.2012.04.017.

[51] P. Zambrano, M. Manrique-Moreno, K. Petit, J.R. Colina, M. Jemiola-Rzeminska, M. Suwalsky, K. Strzalka, Differential scanning calorimetry in drug-membrane interactions, Biochem. Biophys. Res. Commun. 709 (2024) 149806, https://doi.org/10.1016/j.bbrc.2024.149806.

[52] D. Marquardt, N. Kučerka, J. Katsaras, T.A. Harroun, α-Tocopherol's location in membranes is not affected by their composition, Langmuir 31 (2015) 4464–4472, https://doi.org/10.1021/la502605c.

[53] K.L. Koster, M.S. Webb, G. Bryant, D.V. Lynch, Interactions between soluble sugars and POPC (1-palmitoyl-2-oleoylphosphatidylcholine) during dehydration: vitrification of sugars alters the phase behavior of the phospholipid, Biochim. Biophys. Acta Biomembr. 1193 (1994) 143–150, https://doi.org/10.1016/0005-2736(94)90343-3.

[54] W.C. Mobley, H. Schreier, Phase transition temperature reduction and glass formation in dehydroprotected lyophilized liposomes, J. Control. Release 31 (1994) 73–87, https://doi.org/10.1016/0168-3659(94)90082-5.

[55] K. Czamara, K. Majzner, M.Z. Pacia, K. Kochan, A. Kaczor, M. Baranska, Raman spectroscopy of lipids: a review, J. Raman Spectrosc. 46 (2015) 4–20, https://doi.org/10.1002/jrs.4607.

[56] C.J. Orendorff, M.W. Ducey Jr., J.E. Pemberton, Quantitative correlation of Raman spectral indicators in determining conformational order in alkyl chains, J. Phys. Chem. A 106 (2002) 6991–6998, https://doi.org/10.1021/jp014311n.

[57] F.N.R. Petersen, C.H. Nielsen, Raman spectroscopy as a tool for investigating lipid protein interactions, Spectroscopy 24 (2009) 26–35.

[58] R. Gharib, L. Auezova, C. Charcosset, H. Greige-Gerges, Effect of a series of essential oil molecules on DPPC membrane fluidity: a biophysical study, J. Iran. Chem. Soc. 15 (2018) 75–84, https://doi.org/10.1007/s13738-017-1210-1.

[59] K. Gardikis, S. Hatziantoniou, K. Viras, M. Wagner, C. Demetzos, A DSC and Raman spectroscopy study on the effect of PAMAM dendrimer on DPPC model lipid membranes, Int. J. Pharm. 318 (2006) 118–123, https://doi.org/10.1016/j.ijpharm.2006.03.023.

[60] R.K. Singh, S.N. Singh, B.P. Asthana, C.M. Pathak, Deconvolution of lorentzian Raman linewidth: techniques of polynomial fitting and extrapolation, J. Raman Spectrosc. 25 (1994) 423–428, https://doi.org/10.1002/jrs.1250250608.

[61] S. Xia, C. Tan, Y. Zhang, S. Abbas, B. Feng, X. Zhang, F. Qin, Modulating effect of lipid bilayer–carotenoid interactions on the property of liposome encapsulation,

Colloids Surf. B: Biointerfaces 128 (2015) 172–180, https://doi.org/10.1016/j.colsurfb.2015.02.004.
[62] J. Giancaspro, P. Scollan, J. Rosario, E. Miller, S. Braziel, S. Lee, Structural determination of model phospholipid membranes by Raman spectroscopy: laboratory experiment, Biochem. Mol. Biol. Educ. 50 (2022) 181–192, https://doi.org/10.1002/bmb.21603.
[63] D. Kashchiev, D. Exerova, Bilayer lipid membrane permeation and rupture due to hole formation, BBA-Biomembranes 732 (1983) 133–145, https://doi.org/10.1016/0005-2736(83)90196-7.